

Amplitude Amplification and Estimation using quantum kicked rotor

Keshav. V* and M. S. Santhanam†

Indian Institute for Science Education and Research Pune

Dr. Homi Bhabha Road, Pune 411 008, India.

(Dated: June 21, 2024)

The quantum kicked rotor (QKR) had been widely used for studying quantum chaos and the physics of Anderson localization. It is shown that QKR can be used to design a quantum algorithm to perform unstructured search. This is illustrated through amplitude amplification, a generalization of Grover’s search algorithm, using QKR system. Further, QKR is employed for amplitude estimation when the amplitude of the marked states is unknown. It is also shown that dynamical localization in QKR can be exploited to enhance the performance of the amplitude amplification algorithm by reducing the average runtime. The sensitivity of the success probability of unstructured search to detuning from resonance and the effects of noisy kick strengths are analyzed and the robustness of the QKR based algorithm is shown. The experimental feasibility of every component of the algorithm is discussed.

I. INTRODUCTION

Amplitude Amplification is one of the versatile and popular technique that powers quantum algorithms [1]. It is a deterministic scheme to systematically selectively amplify the amplitudes of known or unknown states, starting from an initial superposition state. It is based on a generalization of Grover’s algorithm for unstructured database search [2], and is a prototypical example that gives a quadratic speedup over the best classical algorithm. Grover’s original algorithm proposed a specific scheme to enhance the amplitudes of the “marked” states, involving repeated applications of a multi-qubit Hadamard gate and the Grover oracle. However, it was subsequently realized [3] that the Hadamard gate could be substituted with almost any unitary to amplify amplitudes provided that there is a scheme for implementing the Grover oracle and time-reversed dynamics. In this generalised framework, an extra step of amplitude estimation is also required [1] to estimate the number of iterations of the algorithm.

Over the years, Grover’s algorithm has been experimentally implemented in various test-beds. The first implementation utilized nuclear magnetic resonance system with 4-qubits [4], while a later attempt significantly improved the efficiency of readout [5]. Other significant implementations include a 2-qubit experiment based on trapped atomic ions [6, 7], using a system of superconducting two coupled transmon qubits [8], and through a one-way quantum computing paradigm using polarization states of photons [9], and more recently a variant of Grover was realized with linear optical system [10, 11]. Further, a classical implementation in Fourier optics setup shows that quantum speedup can be realized in a far-from-quantum regime [12]. In many of these platforms, there is usually a compromise between scalability

and control. Experimentally controlling larger number of qubits is a challenge, and hence scalability of the system size is dependent on the ability to control the collection of qubits. In this article we propose a scheme to efficiently implement amplitude amplification and estimation using the quantum kicked rotor (QKR) and argue that it is well suited to overcome some of these challenges.

The one-dimensional kicked rotor is a paradigmatic model of Hamiltonian chaos and has been extensively investigated in the last five decades [13]. It can be thought of as the dynamics of a free particle on a ring that is periodically kicked by an external sinusoidal field. For sufficiently strong kicks, this system displays classical chaos even as the particle absorbs unbounded energy. In contrast, in the corresponding quantum regime, the energy absorption is arrested by quantum interferences resulting in the localization in momentum space. This emergent phenomenon, termed dynamical localization, is the momentum space analogue of Anderson localization, and has been experimentally observed in laser-kicked cold atomic cloud and in dilute Bose-Einstein condensates []. For the present purposes in this work, parameters must be chosen such that dynamical localization in QKR is avoided. This is achieved through quantum resonance, i.e, by tuning the kick period T to its resonant value T_r such that the free evolution between consecutive kicks becomes an identity operation. For this special case of quantum resonance with $T = T_r$, as proposed and experimentally demonstrated in Refs. [14–17], the dynamics induced by QKR is identical to that of a walker in a tight-binding lattice executing a continuous-time quantum walk with cosine kick potential. In this scenario, the mean energy does not localize, but instead displays a ballistic growth : $\langle E \rangle \sim t^2$.

The connection between QKR at resonance and continuous time quantum walk has been exploited to demonstrate a search protocol on momentum lattice using Bose-Einstein condensates kicked by an optical lattice [17]. This scheme suffers from the following drawbacks – the final probability (before measurement) is quite small ~ 0.1 , and translates to poor fidelity of the search result.

* keshav.v@students.iiserpune.ac.in

† santh@iiserpune.ac.in

Secondly this scheme involves only one oracle implementation and cannot be mapped to the known optimal quantum algorithm (such as due to Grover) for the same procedures. Since the quadratic speedup in Grover's search is optimal [18], the scheme reported in Ref. [17] would not be able to yield a good fidelity without a number of oracle calls quadratic in the number of elements involved in the search.

In this work, we propose a search scheme based on QKR at resonance that overcomes these issues and, importantly, can be mapped to amplitude amplification and Kitaev's phase estimation protocols. As demonstrated in a later section, this leads to good fidelity of the search result. We begin by recalling the connection of the QKR to continuous-time quantum walks in Sec. II. In Sec. III, implementation of the QKR-based unitary gates required for amplitude amplification is discussed, a procedure for amplitude amplification is outlined. The loss of quadratic speedups and ways to resolve this are discussed in Sec. III A, alongside a scheme for amplitude estimation in Sec. IV. The effects of common errors on the fidelity of the algorithm is discussed in Sec. V-VI. Finally, in Sec. VII, some potential generalizations to similar kicked systems as well as the experimental protocols are discussed.

II. QUANTUM KICKED ROTOR

The Hamiltonian of a QKR is given by

$$\hat{H} = \frac{L^2}{2I} + \phi V(\theta) \sum_{j=0}^{\infty} \delta(t - jT), \quad (1)$$

where θ and L represent, respectively, the angle (position) and angular momentum of the rotor, and $I = 1$ its moment of inertia. Further, T is the time period of the kicks, ϕ is the kick strength, and $V(\theta)$ is the kick potential. It describes the dynamics of a periodically kicked particle on a ring implying periodic boundary condition in position alone. In a later section, we employ an additional internal spin- $\frac{1}{2}$ degree of freedom (in the form of two hyperfine states), which is necessary for achieving phase kickbacks for the amplitude estimation. Usually, $V(\theta)$ is chosen to be a single cosine function, but in this work different periodic functions will be used which could be represented as linear combination of cosines and sines. Since Eq. 1 is periodic in time, the dynamics of QKR can be conveniently studied by using a Floquet operator

$$U_{kr} = U_{kick} U_{free} = \exp(-\phi V(\theta)/\hbar_s) \exp(-L^2/2\hbar_s), \quad (2)$$

which evolves an arbitrary initial state for one full time period starting from just after a kick ending just before the next kick. In this, $\hbar_s = T\hbar$ is the scaled Planck's constant. When the kick period T is not tuned to its resonant value T_r , then QKR exhibits dynamical localization in momentum space. As shown by Fishman, Grempe and Prange[19], through a nonlinear transformation

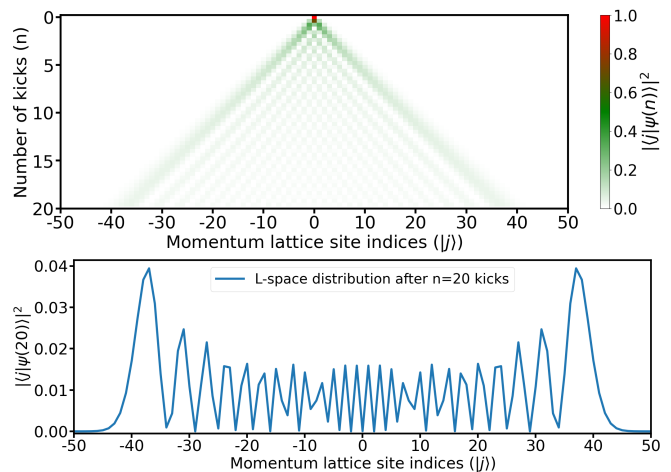


FIG. 1. Dynamics of quantum kicked rotor under conditions of quantum resonance with kick strength $\phi=2$. (a) space-time density plot over momentum lattice points, and (b) density profile at $t = 20$ over momentum lattice. This clearly resembles that of a continuous-time quantum walk.

Eq. 2 can be mapped to a Anderson-type model with diagonal disorder and short-range hopping probabilities. In the light of this correspondence, the dynamical localization in momentum space of QKR is understood to be similar to the Anderson localization. Thus, dynamical localization displays similar signatures as Anderson localization, *e.g.*, exponential profile of evolving wavefunction. By now, it is well appreciated that Anderson localization is a generic feature of wave propagation in disordered media [20].

In contrast, if we choose T such that $\hbar_s = \hbar T = 4\pi$ (condition for quantum resonance), then the free evolution operator becomes an identity operator, and time evolution generated by the unitary operator

$$U = U_{kick} = e^{-\phi V(\theta)/\hbar_s} \quad (3)$$

just imprints a phase on the evolving wavefunction at every time step. Then, it can be shown that a ballistic growth in the mean energy with time is also observed. As is usually done, in this work, $\hbar = 1$ and the kick period T is tuned to for resonance condition. It might be noted that if $V(\theta) = \cos \theta$, then the resonant QKR generates a continuous-time random walk in the momentum space of an infinite path graph with each node being an eigenstate of the angular momentum operator [17].

This property is useful in generating an initial state that is approximately a uniform superposition of basis states. Figure 1(a) shows the space-time plot for a quantum walk generated by the kicked rotor Hamiltonian Eq. 1 at resonance. The profile has the familiar conical shape reflecting that the standard deviation of the walk is $\propto t$, and is similar to that for CTQW. As seen in 1(b), the probability distribution over momentum space at $t = 20$ is quite rugged as is consistent with that expected for a CTQW. In principle, it would be possible to implement

the amplitude amplification algorithms with almost any kick potential, but a quadratic speedup can be realized only when the amplitudes of initial state are reasonably uniform in magnitude.

III. QKR FOR AMPLITUDE AMPLIFICATION

In this section, we will discuss an algorithm for amplitude amplification using the QKR dynamics at resonance. The first step of the Grover's algorithm is to produce an initial state that is uniformly distributed over the computational basis, and this is usually achieved by application of Hadamard operators. In the generalized amplitude amplification algorithm, we should be able to perform the following steps using QKR unitary operators; (a) Hadamard can be replaced with any unitary U that will also produce a uniform superposition, (b) a method for marking sites by implementing the Grover oracle and (c) the ability to execute time-reversed dynamics U^\dagger . These steps can be stated as an algorithm as follows :

In the following subsections, we deal with each one of these requirements. Note that steps 4-6 in this algorithm together constitute the Grover diffusion operation.

A. Creating an optimal initial distribution

In principle, the proposed algorithm could be implemented using a cosine kick potential, and we could mark any momentum state of choice. However, in practise, this may not always produce a quadratic speedup because U , in Eq. 3, with $V(\theta) = \cos \theta$ produces a highly non-uniform probability distribution in momentum space. If the marked site has low amplitude, the number of iterations required for its amplification, and the average runtime might not have the \sqrt{N} scaling. Furthermore, even if the number of marked sites is known, their identities are not. It is then not possible to know the required number of iterations, which depends on the amplitudes of the marked states. For these reasons, it is necessary to make the initial distribution as close to uniform as possible. We present two possible approaches to generate near-uniform initial state.

Modified potential approach: Numerically, we find that kick potentials of the form

$$V(\theta) = \sum_{n=1}^m \frac{\cos n\theta}{n^2} \quad (4)$$

produce a near-uniform distribution with fluctuations that become smaller for $m \gg 1$. Moreover, marking multiple sites might allow the fluctuations in amplitudes of individual sites about the mean to average out, and this in turn might allow for quadratic speedup to be realized. The momentum-space probability density profile for this scenario with $m = 100$ is shown in Fig. 2 while

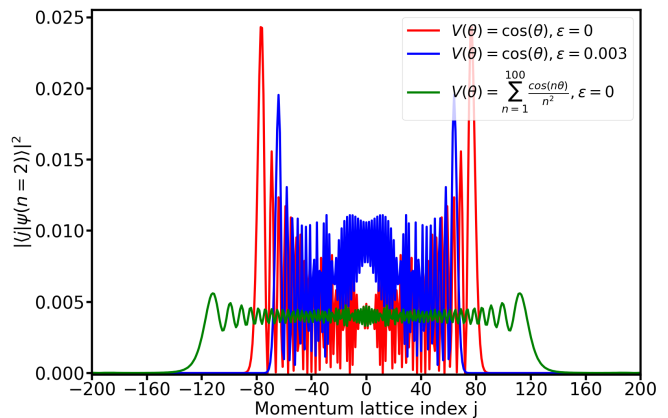


FIG. 2. Initial probability distributions in momentum space for the resonant QKR, when there is a slight detuning from resonance, and with the modified kick potential after 2 kicks. The initial profile obtained using the modified potential looks closer to a uniform distribution and spreads out more than in the other 2 cases after the same number of kicks.

the amplitude amplification procedure performed using the modified kick potential is visualized in Fig. 4.

Approach via controlled detuning: If detuning from resonance can be precisely controlled, it is possible to engineer an initial momentum-space probability distribution that is more uniform than the one which results from applying resonant kicks alone. The rotor must be allowed to evolve freely in a pre-determined and controlled way in the forward cycle, and the order of the free evolution and the kicks must be reversed in each backward evolution cycle in order to execute time-reversal. This technique was also used previously to achieve Loschmidt cooling by means of time-reversal[21]. The operator U , representing forward evolution caused by two non-resonant kicks, is given by

$$U = e^{-i\phi \cos(\theta)} e^{\frac{-iL^2 \epsilon}{2\hbar}} e^{-i\phi \cos(\theta)}. \quad (5)$$

We denote the detuning from resonance by $\epsilon \ll 1$. The term between the two kicks corresponds to free evolution for time interval ϵ , and it prevents the wave-packet from spreading out after the first kick. For $\epsilon \gg 0$, the wave packet localizes in momentum space, well-known phenomenon effect due to dynamical localization. On the other hand, if ϵ is kept small, the wave packet will spread less than it would have in the resonant case, but the momentum-space probability density profile would be more uniform, as shown in Fig. 2, while the amplitude amplification procedure, performed by controlling the detuning is visualized in Fig. 3. From an experimental perspective, the approach through controlled detuning is achievable compared to creating a modified potential of the form in Eq. 4 (especially with large values of m).

B. Implementing the Grover Oracle

It is possible to mark sites (momentum states p) by shifting their phase by π . This allows for an implementation of the Grover oracle, which is a unitary operator that encodes the boolean function $f : \{-N, -N + 1, \dots, N - 1, N\} \mapsto \{0, 1\}$. The function takes the value 1 for all marked states and 0 for all unmarked ones. The corresponding oracle's action on momentum eigenstates must be $O|p\rangle = (-1)^{f(p)}|p\rangle$. The marked states $|p\rangle$ are the ones which have $f(p) = 1$ and are said to span the good subspace.

C. Implementing the Grover Diffusion operator

Grover diffusion operator consists of forward and reversed evolution, and the latter can be implemented by simply shifting the phase of the kicking potential $V(\theta) = \cos\theta$ whilst the system is tuned to resonance. Previously, this property was used for interferometry [22] and to study the effects of quasi-momenta on resonant dynamics [23]. We will use a periodic potential expressed in the Fourier basis as $V(x) = \sum_{n=0}^{\infty} a_n \cos(nx)$. For the time-reversed part of each cycle, each term in this series would have to be individually phase-shifted. Alternatively, the sign of the kick strength ϕ could be changed to achieve time-reversed evolution. With this, the Grover diffusion cycle is described by

$$D = e^{-i\phi V(x)} (1 - 2|0\rangle\langle 0|) e^{i\phi V(x)} = 1 - 2|\psi\rangle\langle\psi|. \quad (6)$$

This can be interpreted as a reflection about the vector orthogonal to $|\psi\rangle$ in the subspace spanned by its normalized projections onto the so-called good and bad subspaces. The crucial factor is that the dynamics generated by U can be easily reversed by changing the sign of ϕ . This procedure is identical to the amplitude amplification technique except for an overall global phase shift π applied in each iteration, which does not affect the success probability. We present our proof of correctness along the same lines as amplitude amplification [1]. Consider a Hilbert space of orthonormal set of states $\{|n\rangle\}$. The good (marked) and bad (unmarked) subspaces are defined in terms of a Boolean function $\chi(n)$ such that $\chi(n) = 1$ indicates marked and $\chi(n) = 0$ unmarked subspaces. Let $|\psi\rangle$ represent a state residing in this space, and is obtained from $|0\rangle$ through

$$|\psi\rangle = e^{-i\phi V(x)} |0\rangle = U |0\rangle. \quad (7)$$

This, in turn, can be expressed as

$$|\psi\rangle = (P_G + P_B) |\psi\rangle = |\psi_1\rangle + |\psi_0\rangle, \text{ and } a = \langle\psi_1|\psi_1\rangle, \quad (8)$$

where P_G and P_B are the projectors onto the good and bad subspaces respectively. We assume that only a finite number of states will be marked, which means that the good subspace $\{|g\rangle\}$ is finite dimensional while the

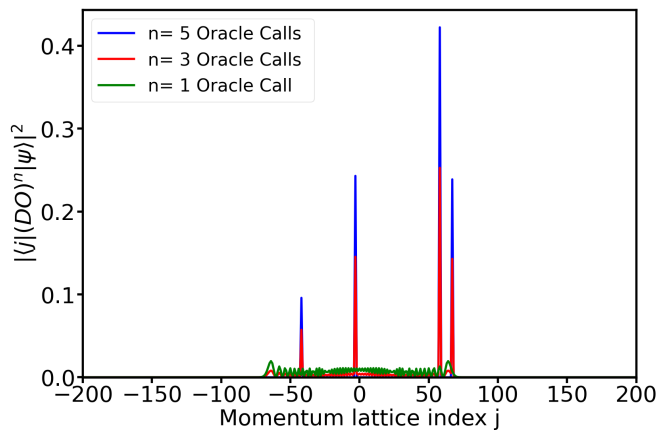


FIG. 3. Amplitude Amplification procedure visualized. The initial distribution is optimized by performing kicks with non-zero detuning from the resonant kick period, with the free evolution being reversed during backward evolution.

bad subspace $\{|b\rangle\}$ is not. The Grover operator, which represents one-iteration of the amplitude amplification process, is defined as

$$G = U^\dagger O_0 U O = (1 - 2|\psi\rangle\langle\psi|)(1 - 2P_G), \quad (9)$$

in which the operators O and O_0 mark the good states and the $|0\rangle$ state respectively. It can be interpreted as a reflection about the projection of $|\psi\rangle$ onto $\{|g\rangle\}$ followed by a reflection about the vector orthogonal to $|\psi\rangle$. Clearly, even after multiple iterations, the dynamics are restricted to the subspace spanned by the vectors $|g\rangle = \frac{|\psi_1\rangle}{\sqrt{a}}$ and $|b\rangle = \frac{|\psi_0\rangle}{\sqrt{1-a}}$. We also define $\theta = \sin^{-1}(\sqrt{a})$. The action of a single Grover iteration on the state vector would be the following.

$$G|\psi\rangle = U^\dagger O_0 U O |\psi\rangle = -\sin\left(\frac{3\theta}{2}\right)|g\rangle - \cos\left(\frac{3\theta}{2}\right)|b\rangle \quad (10)$$

After r iterations, the state would become

$$|\psi^r\rangle = (-1)^r (-\sin((2r+1)\theta)|g\rangle - \cos((2r+1)\theta)|b\rangle). \quad (11)$$

Therefore, we must measure the momentum after

$$r = \left\lceil \frac{\pi}{4\sin^{-1}(\sqrt{a})} - \frac{1}{2} \right\rceil \quad (12)$$

iterations of the Grover operator. If the initial state in Eq. 7 is uniformly distributed in the momentum space, then the probability a for obtaining a marked site will be a good approximation to the fraction of marked sites. In this case, $r \approx \frac{\pi\sqrt{N}}{4\sqrt{M}}$, indicating that quadratic speedup has been obtained.

The expected speedup can be estimated as follows: the initial distribution over momentum sites in Fig. 2 is nearly uniform, and let Σ denote its standard deviation about the mean. Assuming that it truncates sharply

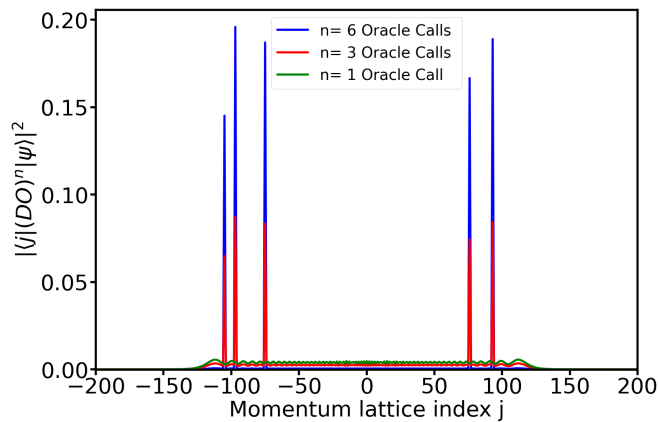


FIG. 4. Amplitude amplification using the modified kick potential. Our numerical results indicate that when multiple sites are marked, the exact quadratic speedup predicted by Grover's formula with $N = \sqrt{3}\sigma$ can be achieved in this case.

beyond $\sqrt{3}\Sigma$, the number of search sites is taken to be $N = 2\sqrt{3}\Sigma$. We found that the expected number of iterations required for a search scales as \sqrt{N} . The lowest green curves in Figs.3, 4 are depicted in Fig.2 in more detail. Both of the suggested approaches yield lower values of the average runtime, which we define as follows:

$$T_{\text{avg}} = \frac{\sum_{i=-\lfloor\sqrt{3}\sigma\rfloor}^{\lceil\sqrt{3}\sigma\rceil} \left[\frac{\pi}{4 \sin^{-1} \sqrt{a_i}} \right]}{2\sqrt{3}\sigma} \quad (13)$$

We have assumed that the states with reasonably large amplitudes are the ones within a range of $\sqrt{3}\sigma$ of 0, where σ is the standard deviation of the distribution, as this is a property of the uniform distribution. The factor a_i is the probability that a measurement of the angular momentum on the initial state yields state $|i\rangle$.

Our numerical results indicate that the average runtimes normalized by $N = \sqrt{3}\sigma$ for the modified kick potential, detuned rotor, and the tuned rotor increase in the same order.

IV. ESTIMATING THE REQUIRED NUMBER OF ITERATIONS

In this implementation of amplitude amplification, since the marked sites are unknown, it is necessary to a priori determine the factor $\sqrt{a} (= \sin(\frac{\theta}{2}))$ in Eq. 12 for the number of iterations. As the probability distribution in momentum space is not uniform and the indices of the marked sites are unknown, it is not possible to calculate the required number of iterations. However it might be possible to estimate it if we engineer a uniform distribution in the initial time.

It is possible, however, to estimate the same amplitudes, using a variant of Kitaev's phase estimation procedure [24][25], described below. The circuit in Fig. IV represents the whole process and the upper wire represents

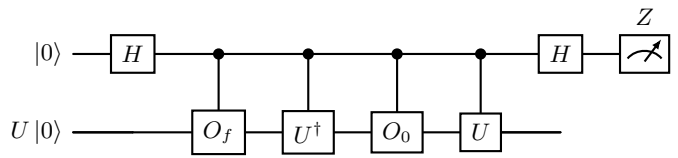


FIG. 5. Circuit for a variant of Kitaev's phase estimation procedure.

the internal hyperfine state while the lower one represents the state on the angular momentum lattice.

Firstly, Hadamard gate is applied to the internal hyperfine state, which can be realized using microwave pulses as described in [14]. The second is the oracle controlled by the internal hyperfine state, and can be implemented using phase gates on the internal state controlled by the momentum-state (if the momentum state is one of the marked ones, the phase gate will be implemented on the internal hyperfine level). The controlled O_f gate can be decomposed as follows :

$$c - O_f = |0\rangle\langle 0| \otimes \mathbb{I} + |1\rangle\langle 1| \otimes O_f = \mathbb{I} \otimes \mathbb{I} - 2|1\rangle\langle 1| \otimes P_G \\ = \mathbb{I} \otimes P_B + Z \otimes P_G = \sum_{n \notin M} \mathbb{I} \otimes |n\rangle\langle n| + \sum_{m \in M} Z \otimes |m\rangle\langle m|$$

The gate in the final expression can be implemented using velocity-selective Raman transitions [26]. In the above, M represents the set of marked momentum states. The controlled versions of the U ,

$$U = e^{-i(\phi_1|1\rangle\langle 1|) \otimes V(\theta)} = |0\rangle\langle 0| \otimes \mathbb{I} + |1\rangle\langle 1| \otimes e^{-i\phi_1 V(\theta)}$$

and U^\dagger can be implemented as special cases of biased DTQWs [27] with bias 1 for the internal state $|1\rangle$. Since biased DTQWs have already been realized in practice [27], this step should be experimentally feasible as well.

The controlled oracle and the diffusion operator together constitute a single iteration of amplitude amplification. On the subspace spanned by $P_G |\psi\rangle$ and $P_B |\psi\rangle$, the action of a single iteration of amplitude amplification is identical to that of a rotation on the same plane, whereas for any vector in the subspace orthogonal to it, the amplitude amplification unitary acts as the identity. The state $|\psi\rangle$ can be expressed as a linear combination of two eigenvectors of the amplitude amplification unitary, $|\pm\rangle$, with eigenvalues $-e^{\pm i\theta}$. In the following we denote the

controlled version of Amplitude Amplification by cA .

$$\begin{aligned}
 |\psi\rangle &= \sin\left(\frac{\theta}{2}\right) |s\rangle + \cos\left(\frac{\theta}{2}\right) |w\rangle = \frac{ie^{-i\theta/2}}{\sqrt{2}} |+\rangle - \frac{ie^{i\theta/2}}{\sqrt{2}} |-\rangle \\
 |s\rangle &= \frac{P_G |\psi\rangle}{\langle \psi | P_G | \psi \rangle}, |w\rangle = \frac{P_B |\psi\rangle}{\langle \psi | P_B | \psi \rangle}; |\pm\rangle = \frac{\pm i |s\rangle + |w\rangle}{\sqrt{2}} \\
 |\psi_2\rangle &= cA(|+\rangle \otimes |\psi\rangle) = cA\left(\frac{|0\rangle + |1\rangle}{\sqrt{2}}\right) \left(\frac{ie^{-i\theta/2}}{\sqrt{2}} |+\rangle - \frac{ie^{i\theta/2}}{\sqrt{2}} |-\rangle\right) \\
 &= \frac{1}{2} \left(ie^{-i\theta/2} |0\rangle |+\rangle - ie^{i\theta/2} |0\rangle |-\rangle - ie^{i\theta/2} |1\rangle |+\rangle + ie^{-i\theta/2} |1\rangle |-\rangle \right)
 \end{aligned}$$

The measurement outcome after applying another Hadamard operation to the internal qubit is identical to the one we would get if we measured X right away after receiving the phase kickback, since $HZH = X$. The expected value of the measurement in the Z basis is $\langle \psi_2 | X | \psi_2 \rangle = -\cos(\theta)$ where θ is the angle we must estimate to know the number of iterations of the amplitude amplification required. Thus, by performing many iterations of this algorithm, it is possible to estimate θ upto any desired level of precision. Ideally, this should be done prior to the search algorithm to obtain the necessary number of iterations.

V. EFFECTS OF ERRONEOUS DETUNING FROM RESONANCE

The reason for tuning the QKR system to resonance are twofold: Firstly, a resonant kicked rotor will not exhibit dynamical localization. Instead, the momentum-space wave-packet displays a ballistic spread, and a superposition is created fairly quickly. In the present case, the mean energy evolves as $\langle E \rangle \sim t^2$. The second advantage is that the resonant dynamics can be reversed by simply shifting the phase of the kick potential. However, even a small (uncontrolled) detuning from resonance will make the dynamics irreversible. Erroneous detuning from resonance might be relevant if the marking process employed is slow, in which case the undesired free evolution of QKR during the marking step must also be accounted for. The forward and backward kick sequences are given by the following expressions :

$$U_f = e^{-\frac{iL^2\epsilon}{2\hbar}} e^{-i\phi_a \cos(\theta)}; \quad U_b = e^{-\frac{iL^2\epsilon}{2\hbar}} e^{i\phi_a \cos(\theta)}.$$

Each time a kick is imparted, the state is rotated away from the desired state by a small angle due to the free evolution part of the Floquet operator. In this scenario, even if the kick strength alternates between positive and negative values, it is impossible to realize the diffusion operator which requires time-reversed evolution in the form $U_f^\dagger \neq U_b$. Erroneous detuning from resonance leads to errors that build up after each Grover iteration, and could lead to large cumulative errors. This is depicted in Fig. 6.

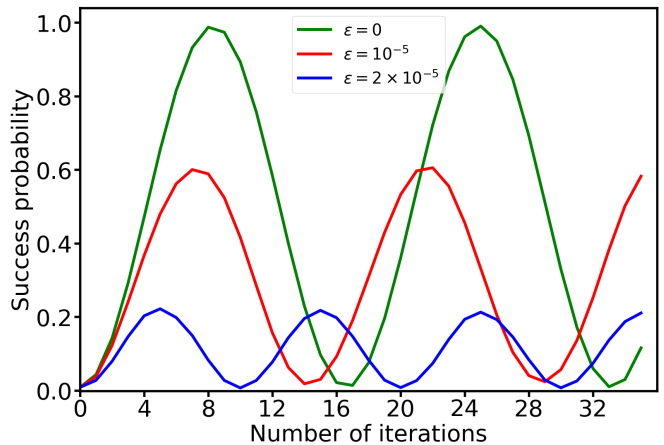


FIG. 6. Success probabilities for different amounts of erroneous detuning from resonance. The fidelity quickly decays as with increasing values of detuning from quantum resonance. Here the reported values ϵ are the values of the detuning normalized by the kick period.

VI. SENSITIVITY TO NOISY KICKS

Adding a stochastic term to the Hamiltonian of a quantum system can lead to a decay in purity when we average over all the trajectories. The classical noise processes can be used to simulate decoherence by means of pure dephasing [28]. This can be implemented in QKR with kick strengths becoming random variable sampled from a normal distribution ($\phi_j \sim N(\phi, \delta)$). We proceed to analyze the sensitivity of the proposed amplitude amplification protocol to noise in the kicks.

This is done by performing the same algorithm using a series of QKR Floquet operators with different kick strengths. These kick strengths are modelled as independent and identical normal random variables. We analyze the sensitivity by checking how the errors scale with the noise-strength, parameterized by the standard deviation of the distribution of the kicks.

A. Noise-averaged dynamics

The noise-averaged density operator can to reproduce the dynamics of expectation values of observables after multiple realizations of the noise, since trace and noise-averaging are commuting linear operations: $\overline{\text{Tr}\{O\rho\}} = \text{Tr}\{O\bar{\rho}\}$. For a sequence of m noisy kicks, the state of the system is

$$\rho(mT^+) = e^{-i\tilde{\phi}V(\theta)} \rho(0) e^{i\tilde{\phi}V(\theta)}; \quad \tilde{\phi} = \sum_{j=1}^m \phi_j. \quad (14)$$

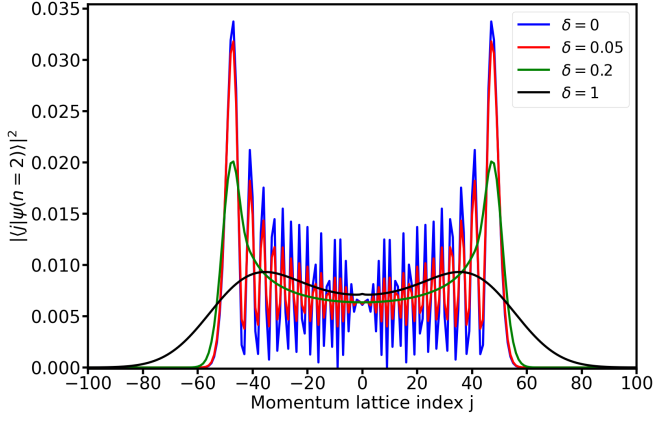


FIG. 7. Noise-averaged probability density profiles for the resonant noisy QKR.

In position representation, we get

$$\begin{aligned} \langle \theta | \rho(mT^+) | \theta' \rangle &= e^{-i\tilde{\phi}(V(\theta) - V(\theta'))} \langle \theta | \rho(0) | \theta' \rangle, \\ \langle \theta | \overline{\rho(mT^+)} | \theta' \rangle &= e^{-im\phi(V(\theta) - V(\theta'))} (F(\theta, \theta'))^m \langle \theta | \rho(0) | \theta' \rangle, \\ F(\theta, \theta') &= e^{-\frac{\delta^2(V(\theta') - V(\theta))^2}{2}}. \end{aligned} \quad (15)$$

This is similar to the result of the addition of a continuous-time stochastic process to the Hamiltonian, which also causes non-unitary evolution of the ensemble-averaged density operator [29]. The momentum space probability density profile for a QKR with the standard cosine kick potential subjected to a few noisy kicks is depicted in Fig. 7. Now, Eq. 15 can be used to compute trace with any observable, resulting in the corresponding noise-averaged expectation value. From Eq. 15, it is also clear that for all $\theta \neq \theta'$, $\theta \neq 2\pi - \theta'$, the matrix element $\langle \theta | \rho(mT^+) | \theta' \rangle = 0$ as long as $V(\theta)$ is invertible in the interval $[0, 2\pi]$. Thus, most of the off-diagonal matrix elements decay exponentially with time, indicating decoherence. The noise-averaged dynamics of the density operator do not differ from the noiseless case to the first order (as seen by Taylor expanding the noise term in Eq. 15).

B. Effects of noisy kicks on Amplitude Amplification

In this, we analyze the sensitivity of the amplitude amplification procedure to noise in the kicks. In the noiseless case, the success probability is an oscillating sinusoidal function of the number of iterations of amplitude amplification. As Fig. 8 shows, the noise-averaged success probability decreases as the noise strength Γ (the standard deviation of the distribution of the kick strength) increases, and the fidelity drops. If averaging over multiple noise realizations is not performed, irregular fluctu-

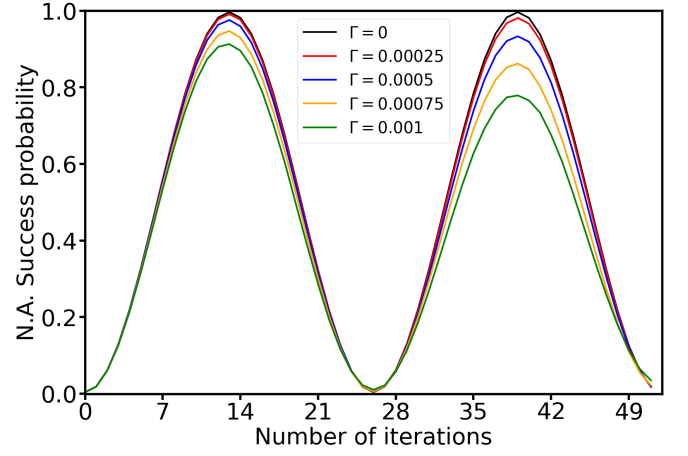


FIG. 8. The plots depict noise-averaged success probabilities after various numbers of iterations of amplitude amplification. The noise strength reported is normalized by the kick strength

ations are observed which usually get smoothed out by averaging over many trajectories.

If a closed-form for evolution of the noise-averaged density operator is found, then the noise-averaged fidelity could be obtained by taking the trace with $P_G = \sum_{m \in M} |m\rangle \langle m|$. The density operator at the $r+1$ th iteration is related to the state after the r th iteration through the following relation:

$$\begin{aligned} \langle \theta | \rho^{r+1} | \theta' \rangle &= \langle \theta | D^r O \rho^r O (D^r)^\dagger | \theta' \rangle, \\ D^r &= e^{-i\delta\phi_{2r}V(\theta)} (\mathbb{I} - 2|\psi_0\rangle \langle \psi_0|) e^{i\delta\phi_{2r-1}V(\theta)}, \end{aligned}$$

where the random variables $\delta\phi_l = \phi_l - \phi$ are independent for all $0 \leq l \leq 2r$. Hence, to obtain full noise averaged result, independently averaging over $\delta\phi_l$ is possible. The relevant calculations are discussed in Appendix A. This can also be shown by explicitly calculating the first order correction due to the noise. Consider the derivative of any coefficient in the expansion of the state vector after N iterations of amplitude amplification :

$$\begin{aligned} |\psi^N\rangle &= \prod_{r=1}^N [e^{-i\delta N_{2r}V(\theta)} (\mathbb{I} - 2|\psi_0\rangle \langle \psi_0|) \\ &\quad e^{i\delta N_{2r-1}V(\theta)} (\mathbb{I} - 2P_G)] |\psi\rangle. \end{aligned}$$

We use the fact that $\delta\phi_l = \delta N_l \sim \delta N(0, 1)$ since N_l is a normal random variable. Now, by expanding the state vector in the angular momentum eigenbasis $|\psi^N\rangle = \sum_{n \in \mathbb{Z}} c_n(\delta) |n\rangle$, the derivative of c_n with respect to δ , at $\delta = 0$, has the following expression:

$$\begin{aligned} \frac{dc_n(\delta)}{d\delta} &= i \sum_{r=1}^N \langle n | G^{N-r} \left[-N_{2r}V(\theta)G + \right. \\ &\quad \left. N_{2r-1}(\mathbb{I} - 2|\psi_0\rangle \langle \psi_0|)V(\theta)(\mathbb{I} - 2P_G) \right] G^{r-1} |\psi\rangle. \end{aligned}$$

However, $\langle N_l \rangle = 0 \forall 0 \leq l \leq 2N$. Thus, the noise-averaged first order correction (in the noise strength δ) to

the success probability vanishes. On the other hand, the second order correction is non-zero. On similar grounds, it can be argued that all odd-order corrections would evaluate to zero, since all odd moments of the variables N_l are zero, leaving only even-order corrections.

Since the noise-averaged corrections scale as δ^2 to the lowest order, our procedure can be said to be reasonably robust to noise in the kick strengths. Fig.8 indicates that the maximum fidelity decays with an increase in noise strength Γ , where the reported values are rescaled by the kick strength. However, the sensitivity to the noise is much lower than the sensitivity to errors in detuning, where the latter are rescaled by the kick period. We see from Fig.8 and Fig.6 that comparable values of fidelity occur at $\Gamma \sim 10^{-3}$ and rescaled detuning $\epsilon \sim 10^{-5}$ indicating that the Amplitude Amplification procedure is much more robust to noisy kicks than a fixed erroneous detuning from resonance.

The deviations in the success probability of the noiseless case, rescaled by Γ^2 , are displayed in Fig.9. These approximate collapse of all the curves indicates that the quadratic scaling prediction holds true. We note that the deviations from the noiseless cases are vanishingly small though it appears large due to scaling by Γ^2 .

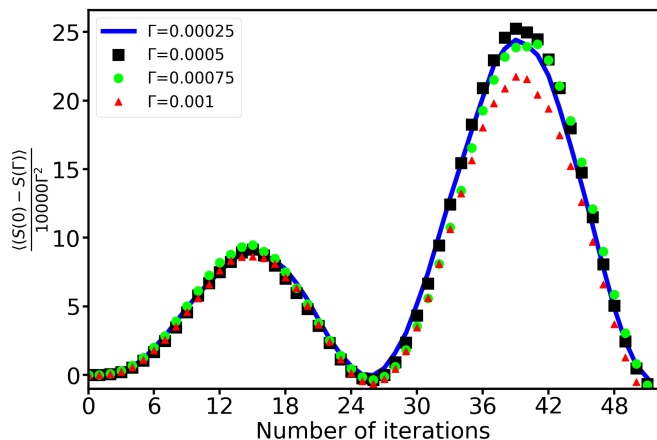


FIG. 9. Deviations of the success probability curves (averaging over multiple noise realizations) for various noise strengths from the noiseless curve, rescaled by a factor Γ^2 have been plotted as functions of number of iterations

VII. CONCLUSIONS AND OUTLOOK

We have presented a scheme for amplitude amplification using standard atom-optics manipulation techniques which can be achieved using a quantum kicked rotor model with an internal spin- $\frac{1}{2}$ degree of freedom. The amplitude amplification algorithm requires three ingredients: (a) a method to implement a unitary operator U not diagonal in the basis of interest, (b) a method for implementing time-reversal of the dynamics caused by U , (c) a method to obtain the phase kickback required

for the Grover oracle. All of these unitary operations can be performed on the kicked rotor, which makes it a suitable platform for the implementation of the algorithm through atom-optics experiments. Thus, the atom-optics kicked rotor is a platform useful for more than just phenomenological studies of quantum chaos and Anderson localization.

In order to obtain an uniformly distributed initial state, we employ a modified kick potential which allows for long-range hopping. Further, a new scheme for amplitude estimation for the quantum kicked rotor has been proposed. Finally, we study the effects of noise on the kick strengths, as well as a fixed (undesired) detuning from quantum resonance condition. Since the variant of kicked rotor employed here is not quantum chaotic, it is of interest to study if a quantum chaotic system can be algorithmic purposes, and whether this will have any advantage over other platforms for computation.

Our proposals are rooted in viable techniques already realized in experiments. The periodic boundary conditions for the spatial degree of freedom could be achieved using a toroidal non-interacting BEC [30]. The π phase shifts required for marking are performed by exploiting velocity-selective Raman transitions to select certain momentum values corresponding to the lattice sites to be marked and taking the internal 2-level system on an adiabatic cycle which leads to a global geometric phase of π for the internal state. But since this operation is done selectively on certain momentum states, it becomes a relative phase for these alone. Realizing an arbitrary kick potential is certainly possible from the point of view of an experiment since each term in the Fourier series corresponds to a different laser with a different wavelength. We require an operation controlled by the internal state in phase estimation, and such operations might typically be challenging to perform. However, we showed that this operation can be rewritten in terms of momentum-selective phase gates which may once again be implemented using velocity-selective Raman transitions. We expect that the results in this work would lead to experimental realization of amplitude amplification using atom-optics test beds.

VIII. ACKNOWLEDGMENTS

We would like to thank S. Sagar Maurya for multiple discussions about the experimental feasibility of the procedures proposed as well as several useful inputs and suggestions on various other aspects of this work. We would also like to thank J Bharati Kannan, for some suggestions for ways to improve the fidelity of the search protocol. Finally, we would like to thank Professor T.S. Mahesh for a useful discussion about an oracle which makes use of a geometric phase, as well as phase estimation using Kitaev's procedure.

Appendix A: Direct calculation for noise-averaged success probabilities

Using the completeness relation in the $|\theta\rangle$ basis, we obtain the following expression for the average success probability after $r+1$ iterations, in terms of the matrix elements of the noise-averaged state after r iterations.

$$\begin{aligned} \langle \theta | \rho^{\bar{r}+1} | \theta' \rangle &= e^{-\frac{\delta^2(V(\theta)-V(\theta'))^2}{2}} \int_0^{2\pi} d\theta_1 \int_0^{2\pi} d\theta_2 \\ &\langle \theta_1 | D | \theta_1 \rangle \langle \theta_1 | O \bar{\rho}^r O | \theta_2 \rangle \langle \theta_2 | D | \theta' \rangle e^{-\frac{\delta^2(V(\theta)-V(\theta'))^2}{2}} \\ &\langle \theta | D | \theta_1 \rangle = \delta(\theta - \theta_1) - \frac{e^{i(V(\theta_1)-V(\theta))\phi}}{2\pi} \end{aligned}$$

Using the previous expression, the noise-averaged matrix element becomes

$$\begin{aligned} F(\theta, \theta') &\left\{ -\frac{1}{2\pi} \int_0^{2\pi} d\theta_1 e^{i(V(\theta_1)-V(\theta))\phi} \langle \theta_1 | O \bar{\rho}^r O | \theta' \rangle F(\theta, \theta_1) \right. \\ &- \frac{1}{2\pi} \int_0^{2\pi} d\theta_2 e^{i(V(\theta)-V(\theta_2))\phi} \langle \theta | O \bar{\rho}^r O | \theta_2 \rangle F(\theta', \theta_2) + \\ &\left. \frac{1}{4\pi^2} \int_0^{2\pi} d\theta_1 \int_0^{2\pi} d\theta_2 \langle \theta_1 | O \rho O | \theta_2 \rangle e^{i\phi(V(\theta_1)-V(\theta_2))} F(\theta_1, \theta_2) \right. \\ &\left. \langle \theta | O \bar{\rho}^r O | \theta' \rangle F(\theta, \theta') \right\}; F(\theta, \theta') = e^{-\frac{\delta^2(V(\theta)-V(\theta'))^2}{2}} \end{aligned}$$

The success probability after the $(r+1)^{th}$ is related to the state after the r^{th} iteration as follows:

$$\begin{aligned} \text{Tr}\{P_G \rho^{r+1}\} &= \text{Tr}\left\{ \sum_{m \in M} |m\rangle \langle m| \rho^{r+1} \right\} \\ &= \sum_{m \in M} \langle m | e^{-i\delta\phi_2 V(\theta)} (\mathbb{I} - 2|\psi_0\rangle \langle \psi_0|) e^{i\delta\phi_1 V(\theta)} (\mathbb{I} - 2P_G) \\ &\quad \times \rho^r (\mathbb{I} - 2P_G) e^{-i\delta\phi_1 V(\theta)} (\mathbb{I} - 2|\psi_0\rangle \langle \psi_0|) e^{i\delta\phi_2 V(\theta)} |m\rangle \\ &= \sum_{m \in M} \prod_{i=1}^4 \int_0^{2\pi} d\theta_i \langle m | \theta_1 \rangle \langle \theta_1 | (\mathbb{I} - 2|\psi_0\rangle \langle \psi_0|) | \theta_2 \rangle \langle \theta_2 | \\ &\quad \times (\mathbb{I} - 2P_G) \rho^r (\mathbb{I} - 2P_G) | \theta_3 \rangle \langle \theta_3 | (\mathbb{I} - 2|\psi_0\rangle \langle \psi_0|) | \theta_3 \rangle \langle \theta_3 | m \rangle \\ &\quad \times e^{i\delta\phi_{2r}(V(\theta_4)-V(\theta_1))} e^{i\delta\phi_{2r-1}(V(\theta_2)-V(\theta_3))} \end{aligned}$$

After averaging over noise realizations, we obtain the following expression, where the $F(\theta_i, \theta_j)$ factor which accounts for the corrections due to the noise, has the same form as discussed in the previous section.

$$\begin{aligned} &= \sum_{m \in M} \prod_{i=1}^4 \int_0^{2\pi} d\theta_i \frac{e^{im(\theta_4-\theta_1)}}{2\pi} \left[\delta(\theta_2 - \theta_1) \right. \\ &\quad \left. - \frac{2e^{i\phi(V(\theta_2)-V(\theta_1))}}{2\pi} \right] \times \left[\delta(\theta_3 - \theta_4) - \frac{2e^{i\phi(V(\theta_3)-V(\theta_4))}}{2\pi} \right] \\ &\quad \langle \theta_2 | O \rho^r O | \theta_3 \rangle F(\theta_3, \theta_2) F(\theta_4, \theta_1) \end{aligned}$$

Further simplification yields the following sum of 4 terms for the success probabilities, on average. Clearly, the only factor which corrects for noise-related errors (on the average) is $F(\theta_i, \theta_j)$. In the limit of small noise strengths, $F(\theta, \theta') = 1 + \mathcal{O}(\delta^2) \sim 1$. Thus, we may expect that to the first order, the noise would have no effect on the performance of the algorithm, on average.

$$\begin{aligned} \langle n | \rho^{\bar{r}+1} | n \rangle &= T_1 - 2(T_2 + T_3) + 4T_4 \\ T_1 &= \sum_m \int_0^{2\pi} d\theta_1 \int_0^{2\pi} d\theta_2 e^{-\delta^2(V(\theta_1)-V(\theta_2))^2} \\ &\quad \times \frac{e^{im(\theta_2-\theta_1)}}{2\pi} \langle \theta_1 | O \rho O | \theta_2 \rangle \\ T_2 &= \sum_m \int_0^{2\pi} d\theta_1 \int_0^{2\pi} d\theta_3 \int_0^{2\pi} d\theta_4 F(\theta_1, \theta_3) F(\theta_1, \theta_4) \\ &\quad \times \frac{e^{im(\theta_4-\theta_1)}}{2\pi} \frac{e^{i\phi(V(\theta_4)-V(\theta_3))}}{2\pi} \langle \theta_1 | O \rho^r O | \theta_3 \rangle \\ T_3 &= \sum_m \int_0^{2\pi} d\theta_1 \int_0^{2\pi} d\theta_2 \int_0^{2\pi} d\theta_3 F(\theta_1, \theta_3) F(\theta_2, \theta_3) \\ &\quad \times \frac{e^{im(\theta_3-\theta_1)}}{2\pi} \frac{e^{i\phi(V(\theta_2)-V(\theta_1))}}{2\pi} \langle \theta_2 | O \rho^r O | \theta_3 \rangle \\ T_4 &= \sum_m \int_0^{2\pi} d\theta_1 \int_0^{2\pi} d\theta_2 \int_0^{2\pi} d\theta_3 \int_0^{2\pi} d\theta_4 F(\theta_1, \theta_2) F(\theta_3, \theta_4) \\ &\quad \times \frac{e^{im(\theta_4-\theta_1)}}{4\pi^2} \langle \theta_2 | O \rho^r O | \theta_3 \rangle e^{i\phi(V(\theta_2)-V(\theta_1)+V(\theta_4)-V(\theta_3))} \end{aligned}$$

-
- [1] G. Brassard, P. Høyer, M. Mosca, and A. Tapp, Quantum amplitude amplification and estimation (2002).
[2] L. K. Grover, A fast quantum mechanical algorithm for database search (1996), arXiv:quant-ph/9605043 [quant-ph].
[3] L. K. Grover, Phys. Rev. Lett. **80**, 4329 (1998).
[4] I. L. Chuang, N. Gershenfeld, and M. Kubinec, Phys. Rev. Lett. **80**, 3408 (1998).
[5] R. Das, T. Mahesh, and A. Kumar, Chemical Physics Letters **369**, 8 (2003).
[6] K.-A. Brickman, P. C. Haljan, P. J. Lee, M. Acton, L. Deslauriers, and C. Monroe, Phys. Rev. A **72**, 050306

- (2005).
[7] C. Figgatt, D. Maslov, K. A. Landsman, N. M. Linke, S. Debnath, and C. Monroe, Nature Communications **8**, 10.1038/s41467-017-01904-7 (2017).
[8] L. DiCarlo, J. M. Chow, J. M. Gambetta, L. S. Bishop, B. R. Johnson, D. Schuster, J. Majer, A. Blais, L. Frunzio, S. Girvin, *et al.*, Nature **460**, 240 (2009).
[9] P. Walther, K. J. Resch, T. Rudolph, E. Schenck, H. Weinfurter, V. Vedral, M. Aspelmeyer, and A. Zeilinger, Nature **434**, 169 (2005).
[10] S.-C. Wang, Y. Chi, L. Yu, Z. Sun, Q.-P. Su, and C.-P. Yang, Phys. Rev. A **103**, 032413 (2021).

- [11] X. He, W.-T. Zhao, W.-C. Lv, C.-H. Peng, Z. Sun, Y.-N. Sun, Q.-P. Su, and C.-P. Yang, *Opt. Lett.* **48**, 4428 (2023).
- [12] N. Bhattacharya, H. B. van Linden van den Heuvell, and R. J. C. Spreeuw, *Phys. Rev. Lett.* **88**, 137901 (2002).
- [13] M. Santhanam, S. Paul, and J. B. Kannan, *Physics Reports* **956**, 1 (2022), quantum kicked rotor and its variants: Chaos, localization and beyond.
- [14] S. Dadras, A. Gresch, C. Groiseau, S. Wimberger, and G. S. Summy, *Physical Review Letters* **121**, 10.1103/physrevlett.121.070402 (2018).
- [15] S. Dadras, A. Gresch, C. Groiseau, S. Wimberger, and G. S. Summy, *Phys. Rev. A* **99**, 043617 (2019).
- [16] M. Delvecchio, F. Petiziol, and S. Wimberger, *Condensed Matter* **5**, 10.3390/condmat5010004 (2020).
- [17] M. Delvecchio, C. Groiseau, F. Petiziol, G. S. Summy, and S. Wimberger, *Journal of Physics B: Atomic, Molecular and Optical Physics* **53**, 065301 (2020).
- [18] M. Boyer, G. Brassard, P. Høyer, and A. Tapp, *Fortschritte der Physik* **46**, 493–505 (1998).
- [19] S. Fishman, D. R. Grempel, and R. E. Prange, *Phys. Rev. Lett.* **49**, 509 (1982).
- [20] P. W. Anderson, *Phys. Rev.* **109**, 1492 (1958).
- [21] J. Martin, B. Georgeot, and D. L. Shepelyansky, *Phys. Rev. Lett.* **100**, 044106 (2008).
- [22] B. Daszuta and M. F. Andersen, *Phys. Rev. A* **86**, 043604 (2012).
- [23] P. D. McDowall, A. J. Hilliard, M. McGovern, T. Grunzweig, and M. F. Andersen, *New Journal of Physics* **11**, 123021 (2009).
- [24] A. Y. Kitaev, Quantum measurements and the abelian stabilizer problem (1995), arXiv:quant-ph/9511026 [quant-ph].
- [25] I. C. M.A.Nielsen, *Quantum computation and quantum information* (2001), Cambridge University Press:978-0521635035.
- [26] J. Ringot, P. Szriftgiser, and J. C. Garreau, *Phys. Rev. A* **65**, 013403 (2001).
- [27] S. Dadras, A. Gresch, C. Groiseau, S. Wimberger, and G. S. Summy, *Phys. Rev. A* **99**, 043617 (2019).
- [28] B. Gu and I. Franco, *The Journal of Chemical Physics* **151**, 014109 (2019).
- [29] A. Kiely, *EPL (Europhysics Letters)* **134**, 10001 (2021).
- [30] P. Qin, A. Andreanov, H. C. P. HC, and S. Flach, Interacting ultracold atomic kicked rotors: loss of dynamical localization (2017).